Physica Status Solidi (RRL) - Rapid Research Letters

Majority carrier transport in single crystal rutile nanowire arrays

--Manuscript Draft--

Manuscript Number:	pssr.201308296
Full Title:	Majority carrier transport in single crystal rutile nanowire arrays
Article Type:	Rapid Research Letter
Section/Category:	Focus Issue on Functional Oxides
Keywords:	photoconductivity; solvothermal; electrical transient; photoelectrochemical water-splitting; solar cells
Corresponding Author:	Karthik Shankar, Ph.D. University of Alberta Edmonton, Alberta CANADA
Additional Information:	
Question	**Response**
Please submit a plain text version of your cover letter here. Please note, if you are submitting a revision of your manuscript, there is an opportunity for you to provide your responses to the reviewers later; please do not add them to the cover letter.	-see enclosed cover letter-
Corresponding Author Secondary Information:	
Corresponding Author's Institution:	University of Alberta
Corresponding Author's Secondary Institution:	
First Author:	Arash Mohammadpour
First Author Secondary Information:	
Order of Authors:	Arash Mohammadpour
	Samira Farsinezhad
	Benjamin Daniel Wiltshire
	Karthik Shankar, Ph.D.
Order of Authors Secondary Information:	
Abstract:	Monocrystalline n-TiO2 nanowires of the rutile phase (Rtl-NWs) grown by a scalable hydrothermal method constitute a functional oxide nanomaterial with potential applications in photovoltaics, photocatalysts, field emitters and electrochemical battery anodes. Carrier transport in Rtl-NWs is of fundamental importance but has hitherto been inferred indirectly via impedance and intensity-modulated spectroscopic techniques. We report an electron drift mobility of 1.95 x 10^-5 cm2 V-1s-1 in rutile nanowire arrays directly measured using the time-of-flight (TOF) and space charge limited current techniques. In addition, we measure an equilibrium free electron concentration of ~10^14 cm-3 and a trap density of 3.5 x 10^16 cm-3 in rutile nanowires. These results point to the importance of reducing traps to improve charge transport in rutile nanowires.

pss-Header will be provided by the publisher

Majority carrier transport in single crystal rutile nanowire arrays

Arash Mohammadpour [*,1], Samira Farsinezhad [,2], Benjamin D. Wiltshire [**,2], and Karthik Shankar [**,1, 2]**

[1] Department of Electrical and Computer Engineering, University of Alberta, Edmonton, AB, T6G 2V4, Canada
[2] National Institute for Nanotechnology, National Research Council, 11421 Saskatchewan Drive, Edmonton, AB, T6G 2M9, Canada

Received ZZZ, revised ZZZ, accepted ZZZ
Published online ZZZ (Dates will be provided by the publisher.)

Keywords photoconductivity, solvothermal, electrical transient, photoelectrochemical solar cells

* Corresponding author: arash.mohammadpour@ualberta.ca, Phone: +01 780 492 3332, Fax: +01 780 492 1811
** email : bwiltshi@ualberta.ca, Phone: +01 780 492 3332, Fax: +01 780 492 1811
** e-mail : kshankar@ualberta.ca, Phone: +01 780 492 1354, Fax: +01 780 492 1811
** e-mail : samira.farsi@ualberta.ca, Phone: +01 780 492 3332, Fax: +01 780 492 1811

Monocrystalline *n*-TiO_2 nanowires of the rutile phase (Rtl-NWs) grown by a scalable hydrothermal method constitute a functional oxide nanomaterial with potential applications in photovoltaics, photocatalysts, field emitters and electrochemical battery anodes. Carrier transport in Rtl-NWs is of fundamental importance but has hitherto been inferred indirectly via impedance and intensity-modulated spectroscopic techniques. We report an electron drift mobility of 1.95 x 10^{-5} cm^2 $V^{-1}s^{-1}$ in rutile nanowire arrays directly measured using the time-of-flight (TOF) and space charge limited current techniques. In addition, we measure an equilibrium free electron concentration of ~10^{14} cm^{-3} and a trap density of 3.5 x 10^{16} cm^{-3} in rutile nanowires. These results point to the importance of reducing traps to improve charge transport in rutile nanowires.

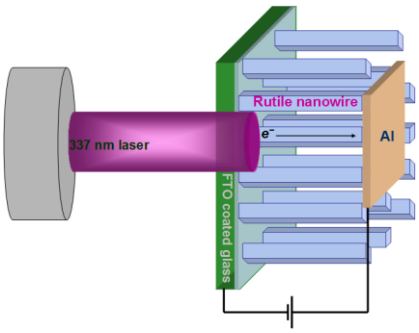

Transient photocurrents in rutile nanowires

1 Introduction TiO_2 is a highly studied transition metal oxide for electronic applications. In nanocrystalline films consisting of sintered anatase nanoparticles, TiO_2 has been used to generate high performance as the electron transporting scaffold in dye-sensitized [1] and bulk heterojunction solar cells [2], as the electron injecting layer in organic light-emitting diodes [3] and active layer in photocatalysts [4, 5]. However, charge transport in nanocrystalline films of titania is known to be highly dispersive and posited to follow a continuous random walk [6-9]. Structural disorder, hopping transport and trapping states are frequently cited as the reasons for dispersive transport.

Improving charge transport in TiO_2 nanostructures has been an enduring goal to improve device performance. In response, one-dimensional nanostructures oriented vertically from the substrate, such as arrays of nanowires and nanotubes, have been synthesized in order to provide vectorial charge percolation paths and thereby prevent a random walk-type of transport [10-12]. Solvothermal-grown rutile nanowire arrays (Rtl-NWs) have the additional advantage of eliminating hopping at grain boundaries due to their monocrystallinity and ensuring band-like transport. Single crystal Rtl-NWs have been used in conjunction with dyes, organic semiconductors and lead halide perovskites to generate high performance solar cells [13-16] and in high-rate photoelectrochemical water-splitting [17]. Rtl-NWs are also attracting research interest as potential lithium ion battery anodes, photocatalysts and field emitters

[18-20]. Therefore, an improved understanding of charge transport in Rtl-NWs is much needed.

In this letter, we present direct measurements of the majority carrier mobility of Rtl-NWs obtained using transient and steady state space charge limited currents (SCLC), and free carrier and trap densities obtained by SCLC.

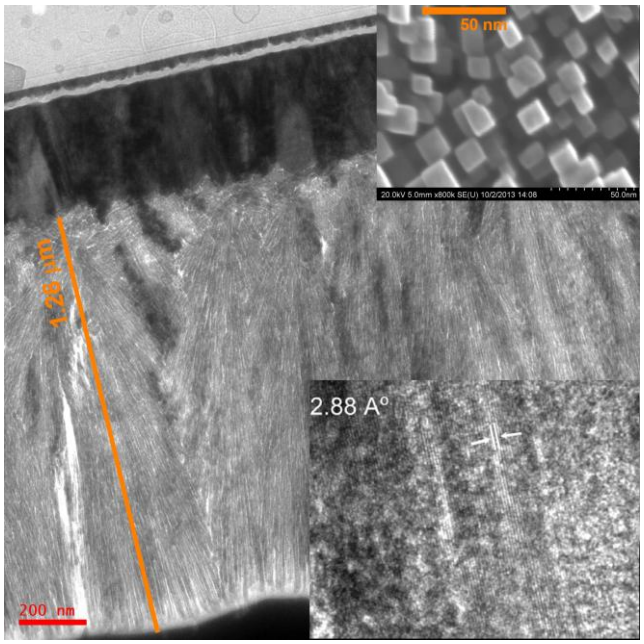

Figure 1 Transmission electron micrograph of the cross-section of rutile nanowire array. One inset (top-right) shows the FESEM top-view of the nanowires and another inset (bottom-right) is the selected area diffraction pattern of the lateral crystal plane of the nanowires.

2 Experimental

2.1 Nanowire synthesis and characterization

Fluorine-doped tin oxide (FTO)-coated glass (TEC-15, 15 ohm/square) substrates were first cleaned with Triton-X detergent followed by thorough rinsing in water, then cleaned in acetone, methanol in an ultrasonic bath and subsequently dried in a nitrogen jet. The substrates were loaded into a 23 mL capacity, sealed Teflon reactor in a PARR acid digestion vessel containing 5 mL of H_2O, 2.5 mL glacial acetic acid and 2.5 mL concentrated HCl. 0.2 mL titanium butoxide was then added drop-by-drop and stirred until a clear solution was obtained The hydrothermal synthesis was performed at 180°C for 6 hours. Morphological and Structural Characterization were performed using a Hitachi S4800 cold field emission scanning electron microscope and a Hitachi HF3300 transmission electron microscope respectively.

2.2 Time-of-flight and SCLC studies Aluminum electrodes were deposited onto the nanowires through a shadow mask in an electron beam evaporation system. The samples were mounted such that deposition occurred at an oblique angle, in order to minimize the depth of penetration of the deposited metal between the nanowires. Voltage bias was applied between the FTO:glass substrate and the aluminum top electrode using a DC power supply. The maximum electric field used was 2 x 10^4 V cm^{-1}. Charge carriers were optically injected into the sample from a nanosecond pulsed N_2 laser (VSL337ND-S, Spectra-Physics) through the FTO:glass substrate which served as the transparent, blocking electrode. Transients were observed using an Agilent DSO1034B sampling oscilloscope using terminal resistances ranging from 50-1000 Ω. To enhance our measurements' signal to noise ratio (SNR), 256 single measurements were averaged, which increased the SNR by a factor of 16. The current-voltage characteristics and capacitance of the samples was measured using a Keithley 4200 semiconductor parameter analyzer equipped with a CVU module.

3 Results and Discussion

As evidenced by Fig. 1, the nanowires are *ca.*1.26 µm in length, vertically oriented from the FTO:glass substrate and 10-20 nm in width. The insets in Fig. 1 show the square facets of the terminal (001) crystal planes and the d-spacing of 0.288 nm corresponding to the (001) crystal plane of rutile, obtained along the length of a nanowire.

Fig. 2 shows the transient photocurrent obtained when the Al top electrode is biased +2 V with respect to the FTO substrate. Under laser illumination through the FTO, most electron-hole pairs are generated within a penetration depth of the transparent contact. For 337 nm radiation, the penetration depth of rutile, given by the inverse of the absorption coefficient, is ~ 200 nm. Photogenerated holes are collected by the closely-lying FTO contact and electrons are injected into the bulk of the nanowires, where they drift under the influence of the applied field (2 x 10^4 V cm^{-1}).

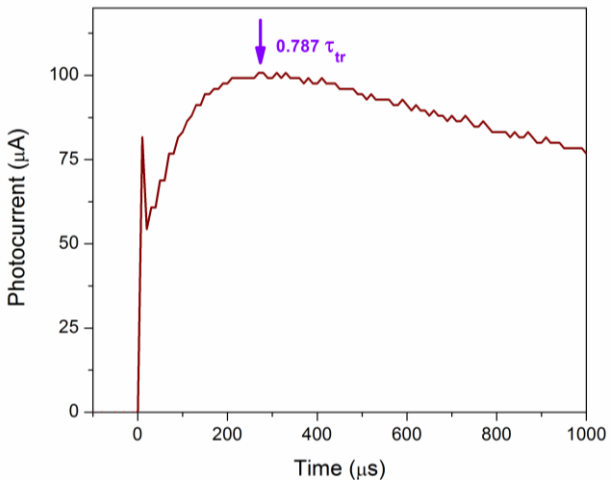

Figure 2 Experimental photoconductivity transient for Rtl-NW array sample with a bias of 2 V (Al-positive and FTO-negative).

By measuring the sample capacitance and by integrating the collected photocurrent, we estimated the injected charge in our experiment Q_{inj} and found it to be much larger than the charge Q_o associated with the geometrical capacitance of the nanowires. Consequently, the excess carrier density is large enough to perturb or modify the electric field inside the nanowires and space-charge limited transport prevails during the drift of electrons through the nanowire. Under these conditions, a cusp is observed in the transient photoconductivity [21], whose temporal location is related to the electron transit time (τ_{tr}) and drift mobility (μ_n) by :

$$t_1 = 0.786 \times t_{tr} = \frac{0.786 L^2}{\mu_n V} \qquad \textbf{(1)}$$

where L is the effective nanowire length over which electron drift occurs and V is the applied voltage bias. Substituting the values of the parameters and the time at which the peak photocurrent occurred in Eq. 1, we obtain an electron mobility of 1.44 x 10^{-5} cm^2 V^{-1}s^{-1}.

The sharp peak at the very beginning of the photoconductivity transient corresponds to the electronic system response time, determined by the series resistance of the oscilloscope and cables, and sample capacitance. The transient photocurrent at the conclusion of the system response peak but still close to the beginning of the transient is approximately half the maximum photocurrent at the cusp. The instantaneous photocurrent density (j_0) at the beginning of the space-charge-limited TOF transient is given by [21] :

$$j_0 = \frac{\varepsilon \mu_n V^2}{2L^3} \qquad \textbf{(2)}$$

where ε is the permittivity of the rutile nanowires. Since the nanowires are oriented along their *c*-axis, a value of 170 was used for the anisotropic relative permittivity of rutile [22, 23]. Using the amplitude of the photocurrent given by Eq. 2, we extract a value of 1.84 x 10^{-5} cm^2 V^{-1}s^{-1} for μ_n. The maximum photocurrent (j_{max}) is expected to overshoot the steady state value by 21% such that j_{max}/j_0 = 2.72. However, the value of j_{max} is less than the value expected from theory due to trapping. The post-transit current in Fig. 2 was fit to a monoexponential decay with a time constant of 1.84 ms.

The *J-V* characteristics of the Rtl-NWs are plotted in Fig. 3, and show distinct transport regimes. At low bias, the slope of the log-log plot is exactly 1 (Region I), corresponding to resistive transport due to the low concentration of mobile charge, the reminder being trapped. As the bias is increased, transport is eventually dominated by electrons injected from the cathode (Region II) and the slope of the plot is 2. As long as the quasi-Fermi level remains lower than the trap level, the ratio θ of free carriers to trapped carriers is a constant independent of bias. The resulting space-charge limited current is given by :

$$j_{SCLC} = \frac{9 \varepsilon \mu_{n,eff} V^2}{8L^3} \qquad \textbf{(3)}$$

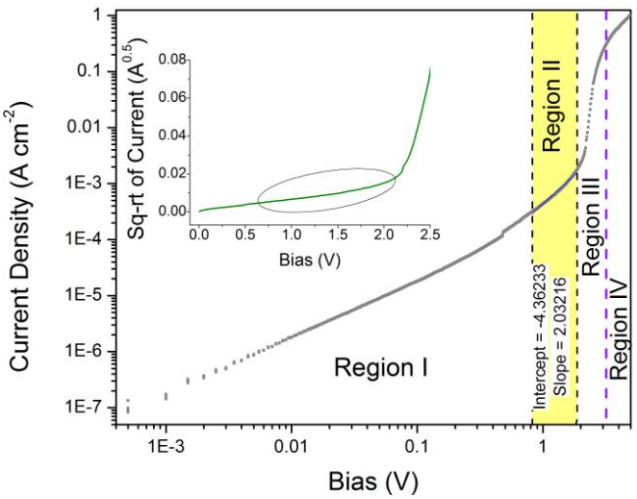

Figure 3 Log-log plot of the steady state current-voltage characteristics of the Rtl-NW array sample. Regions corresponding to different transport regimes are differentiated. The inset is the same *J-V* characteristic plotted on a linear scale with the square root of the current as the y-axis. The ellipse in the inset indicates the space charge limited transport regime where a linear fit is obtained.

where $\mu_{n,eff}$ is the effective electron mobility of a sample with trap-free mobility $\mu_{n,tf}$ in the presence of traps, given by :

$$\mu_{n,eff} = \frac{\theta}{\theta + 1} \mu_{n,tf} \qquad \textbf{(4)}$$

Eq. 3 applied to the SCLC regime (Region II) in Fig. 3 gives a mobility of 2.56 x 10^{-5} cm^2 V^{-1}s^{-1}. Substituting the extracted values of mobility in the linear (resistive) transport regime (Region I), an equilibrium free electron concentration of ≈10^{14} cm^{-3} is obtained for the Rtl-NWs.

As the number of injected carriers increases in Region II, the quasi-Fermi level rises toward the conduction band until it eventually passes through the trap level filling all the traps, thus entering Region III. Above this trap-free limit (V_{TFL}), the current increases rapidly as no further trapping occurs until the injected free charge is approximately equal to the trap density N_T, at which point the current is predominantly composed of mobile charge (Region IV). The trap-free limit is given by [24]

$$V_{TFL} = \frac{eL^2 N_T}{2\varepsilon} \quad (5)$$

From Fig. 3 and Eq. 5, the density of deep traps in the Rtl-NW array sample was extracted to be 3.5 x 10^{16} cm^{-3}.

4. Conclusions

The close correspondence between the electron mobility values extracted from three different techniques provides high confidence in the accuracy of the measurements. The averaged effective electron mobility for rutile nanowires in this letter (1.95 x 10^{-5} $cm^2V^{-1}s^{-1}$) is more than three orders of magnitude lower than the value of 0.1 cm^2 measured in bulk single crystals of reduced rutile [25]. The value of the diffusion coefficient calculated from our measured mobility using the Einstein relation is 3 x 10^{-7} – 7 x 10^{-7} cm^2s^{-1}, which agrees well with the estimates obtained for single crystal rutile NWs by Feng et al [26] from intensity modulated photocurrent and photovoltage spectroscopy (IMPS/IMVS) at low carrier densities. Likewise, Enache-Pommer et al obtained a transport time constant > 1 ms from IMPS in dye-sensitized rutile NWs synthesized by the hydrothermal method [27]. We attribute the difference in mobilities between rutile nanowires and bulk single crystals primarily to trapping states in the bulk and at the surface. Due to the relatively large lateral surface area of the rutile nanowires, dangling bonds and other defects are expected at the surface. In addition, impurity atoms in the nanowires may act as bulk traps. Further studies are planned to understand the nature of trapping states in Rtl-NWs in order to reduce them.

In dye-sensitized and bulk heterojunction Rtl-NW photovoltaics, the large number of electrons injected into the conduction band of rutile by panchromatic absorption of intense AM1.5 sunlight by the sensitizer, will fill traps and result in a higher effective mobility. Therefore, the extracted SCLC-TOF mobility establishes a lower limit for majority carrier transport rates in Rtl-NWs. The measurement of the mobility by SCLC-TOF is also useful because the transport more realistically simulates charge transport in device operating conditions than either field-effect mobility [28] or time-domain terahertz conductivity [29].

Acknowledgements All authors thank NSERC, CFI, Alberta SEGP and NRC for funding/equipment support. AM, SF and BDW acknowledge scholarship support from Alberta Innovates Technology Futures (AITF).

References

[1] S. Ito; S. M. Zakeeruddin; R. Humphry-Baker; P. Liska; R. Charvet; P. Comte; M. K. Nazeeruddin; P. Péchy; M. Takata; H. Miura; S. Uchida; M. Grätzel, *Advanced Materials* **2006,** *18* (9), 1202-1205. DOI 10.1002/adma.200502540.

[2] P. A. van Hal; M. M. Wienk; J. M. Kroon; W. J. H. Verhees; L. H. Slooff; W. J. H. van Gennip; P. Jonkheijm; R. A. J. Janssen, *Advanced Materials* **2003,** *15* (2), 118-121. DOI 10.1002/adma.200390022.

[3] S. A. Haque; S. Koops; N. Tokmoldin; J. R. Durrant; J. Huang; D. D. C. Bradley; E. Palomares, *Advanced Materials* **2007,** *19* (5), 683-687. DOI 10.1002/adma.200601619.

[4] K. Nagaveni; M. S. Hegde; N. Ravishankar; G. N. Subbanna; G. Madras, *Langmuir* **2004,** *20* (7), 2900-2907. DOI 10.1021/la035777v.

[5] J. C. Yu; Yu; Ho; Jiang; Zhang, *Chemistry of Materials* **2002,** *14* (9), 3808-3816. DOI 10.1021/cm020027c.

[6] F. Fabregat-Santiago; G. Garcia-Belmonte; J. Bisquert; A. Zaban; P. Salvador, *The Journal of Physical Chemistry B* **2001,** *106* (2), 334-339. DOI 10.1021/jp0119429.

[7] J. Nelson, *Physical Review B* **1999,** *59* (23), 15374-15380.

[8] J. van de Lagemaat; A. J. Frank, *The Journal of Physical Chemistry B* **2001,** *105* (45), 11194-11205. DOI 10.1021/jp0118468.

[9] A. V. Barzykin; M. Tachiya, *The Journal of Physical Chemistry B* **2002,** *106* (17), 4356-4363. DOI 10.1021/jp012957+.

[10] X. Feng; K. Shankar; O. K. Varghese; M. Paulose; T. J. Latempa; C. A. Grimes, *Nano Letters* **2008,** *8* (11), 3781-3786. DOI 10.1021/nl802096a.

[11] K. Shankar; J. Bandara; M. Paulose; H. Wietasch; O. K. Varghese; G. K. Mor; T. J. LaTempa; M. Thelakkat; C. A. Grimes, *Nano Letters* **2008,** *8* (6), 1654-1659. DOI 10.1021/nl080421v.

[12] K. Zhu; N. R. Neale; A. Miedaner; A. J. Frank, *Nano Letters* **2006,** *7* (1), 69-74. DOI 10.1021/nl062000o.

[13] X. Feng; K. Shankar; M. Paulose; C. A. Grimes, *Angewandte Chemie* **2009,** *121* (43), 8239-8242. DOI 10.1002/ange.200903114.

[14] C. Y. Kuo; W. C. Tang; C. Gau; T. F. Guo; D. Z. Jeng, *Applied Physics Letters* **2008,** *93* (3), -. DOI doi:http://dx.doi.org/10.1063/1.2937472.

[15] H. S. Kim; J. W. Lee; N. Yantara; P. P. Boix; S. A. Kulkarni; S. Mhaisalkar; M. Gratzel; N. G. Park, *Nano Letters* **2013,** *13* (6), 2412-2417. DOI 10.1021/nl400286w.

[16] A. Kumar; A. R. Madaria; C. Zhou, *The Journal of Physical Chemistry C* **2010,** *114* (17), 7787-7792. DOI 10.1021/jp100491h.

[17] G. M. Wang; H. Y. Wang; Y. C. Ling; Y. C. Tang; X. Y. Yang; R. C. Fitzmorris; C. C. Wang; J. Z. Zhang; Y. Li, *Nano Letters* **2011,** *11* (7), 3026-3033. DOI 10.1021/nl201766h.

[18] S. M. Dong; H. B. Wang; L. Gu; X. H. Zhou; Z. H. Liu; P. X. Han; Y. Wang; X. Chen; G. L. Cui; L. Q. Chen, *Thin Solid Films* **2011,** *519* (18), 5978-5982. DOI 10.1016/j.tsf.2011.03.048.

[19] J. M. Wu; H. C. Shih; W. T. Wu, *Chem. Phys. Lett.* **2005,** *413* (4-6), 490-494. DOI 10.1016/j.cplett.2005.07.113.

[20] Y. X. Yu; D. S. Xu, *Appl. Catal. B-Environ.* **2007,** *73* (1-2), 166-171. DOI 10.1016/j.apcatb.2006.07.017.

[21] A. Many; G. Rakavy, *Physical Review* **1962,** *126* (6), 1980-1988.
[22] R. A. Parker, *Physical Review* **1961,** *124* (6), 1719-1722.
[23] M. Dou; C. Persson, *Journal of Applied Physics* **2013,** *113* (8), -. DOI doi:http://dx.doi.org/10.1063/1.4793273.
[24] M. A. Seitz; D. H. Wmtmore, *Journal of Physics and Chemistry of Solids* **1968,** *29* (6), 1033-1049. DOI http://dx.doi.org/10.1016/0022-3697(68)90239-4.
[25] R. G. Breckenridge; W. R. Hosler, *Physical Review* **1953,** *91* (4), 793-802.
[26] X. Feng; K. Zhu; A. J. Frank; C. A. Grimes; T. E. Mallouk, *Angewandte Chemie* **2012,** *124* (11), 2781-2784. DOI 10.1002/ange.201108076.
[27] E. Enache-Pommer; B. Liu; E. S. Aydil, *Physical Chemistry Chemical Physics* **2009,** *11* (42), 9648-9652. DOI 10.1039/b915345d.
[28] M. Katayama; S. Ikesaka; J. Kuwano; Y. Yamamoto; H. Koinuma; Y. Matsumoto, *Applied Physics Letters* **2006,** *89* (24), -. DOI doi:http://dx.doi.org/10.1063/1.2404980.
[29] G. M. Turner; M. C. Beard; C. A. Schmuttenmaer, *The Journal of Physical Chemistry B* **2002,** *106* (45), 11716-11719. DOI 10.1021/jp025844e.